British Journal of Pharmacology

DOI:10.1111/j.1476-5381.2011.01814.x
www.brjpharmacol.org

RESEARCH PAPER

Electrical conduction along endothelial cell tubes from mouse feed arteries: confounding actions of glycyrrhetinic acid derivatives

Erik J Behringer[1], Matthew J Socha[1], Luis Polo-Parada[1,2] and Steven S Segal[1,2]

[1]*Medical Pharmacology and Physiology, University of Missouri, Columbia, MO, USA, and*
[2]*Dalton Cardiovascular Research Center, Columbia, MO, USA*

Correspondence
Steven S Segal, Medical Pharmacology and Physiology, MA415 Medical Science Building, The University of Missouri, Columbia, MO 65212, USA. E-mail: segalss@health.missouri.edu

Keywords
calcium-activated K^+ channels; cell-to-cell coupling; endothelium; gap junction channels; hyperpolarization; microcirculation; resistance arteries

Received
5 August 2011
Revised
29 November 2011
Accepted
7 December 2011

BACKGROUND AND PURPOSE
Electrical conduction along endothelium of resistance vessels has not been determined independently of the influence of smooth muscle, surrounding tissue or blood. Two interrelated hypotheses were tested: (i) Intercellular conduction of electrical signals is manifest in endothelial cell (EC) tubes; and (ii) Inhibitors of gap junction channels (GJCs) have confounding actions on EC electrical and Ca^{2+} signalling.

EXPERIMENTAL APPROACH
Intact EC tubes were isolated from abdominal muscle feed (superior epigastric) arteries of C57BL/6 mice. Hyperpolarization was initiated with indirect (ACh) and direct (NS309) stimulation of intermediate- and small-conductance Ca^{2+}-activated K^+ channels (IK_{Ca}/SK_{Ca}). Remote membrane potential (V_m) responses to intracellular current injection defined the length constant (λ) for electrical conduction. Dye coupling was evaluated following intracellular microinjection of propidium iodide. Intracellular Ca^{2+} dynamics were determined using Fura-2 photometry. Carbenoxolone (CBX) or β-glycyrrhetinic acid (βGA) was used to investigate the role of GJCs.

KEY RESULTS
Steady-state V_m of ECs was −25 mV. ACh and NS309 hyperpolarized ECs by −40 and −60 mV respectively. Electrical conduction decayed monoexponentially with distance (λ ~1.4 mm). Propidium iodide injected into one EC spread into surrounding ECs. CBX or βGA inhibited dye transfer, electrical conduction and EC hyperpolarization reversibly. Both agents elevated resting Ca^{2+} while βGA inhibited responses to ACh.

CONCLUSIONS AND IMPLICATIONS
Individual cells were effectively coupled to each other within EC tubes. Inhibiting GJCs with glycyrrhetinic acid derivatives blocked hyperpolarization mediated by IK_{Ca}/SK_{Ca} channels, regardless of Ca^{2+} signalling, obviating use of these agents in distinguishing key determinants of electrical conduction along the endothelium.

Abbreviations
AFA, abdominal muscle feed artery; βGA, β-glycyrrhetinic acid; $[Ca^{2+}]_i$, intracellular Ca^{2+} concentration; CBX, carbenoxolone; EC, endothelial cell; GA, glycyrrhetinic acid; GJC, gap junction channel; IK_{Ca}/SK_{Ca}, intermediate- and small-conductance Ca^{2+}-activated K^+ channels; K_V, voltage-gated K^+ channels; NS309, 6,7-dichloro-1H-indole-2,3-dione 3-oxime; PSS, physiological salt solution; SMC, smooth muscle cell; SNP, sodium nitroprusside; V_m, membrane potential

Introduction

The role of the endothelium as the principal cellular pathway for signal conduction along the wall of resistance vessels is attributable to the orientation of individual endothelial cells (ECs) along the flow axis and their robust coupling to each other through gap junction channels (GJCs) (Emerson and Segal, 2000b; Looft-Wilson *et al.*, 2004; Wolfle *et al.*, 2007). Once initiated from a local stimulus, the spread of hyperpolarization along the endothelium and into surrounding smooth muscle cells (SMCs) through myoendothelial GJCs promotes vasodilation (Emerson and Segal, 2000a; Bagher and Segal, 2011; Garland *et al.*, 2011; Zhang *et al.*, 2011). As it extends along the intima of arterioles and feed arteries, a single EC makes multiple contacts with ~20 circumferential SMCs through myoendothelial GJCs (Haas and Duling, 1997; Emerson and Segal, 2000a; Sandow *et al.*, 2003). With respect to blood flow control *in vivo*, intercellular conduction along the endothelium from arterioles into proximal feed arteries is essential to ascending vasodilation during exercise. Indeed, as shown in contracting hamster skeletal muscle, interruption of this signalling pathway impairs feed artery dilation, thereby attenuating functional hyperaemia by half (Segal and Jacobs, 2001). A complementary role for intercellular conduction along arteriolar endothelium has been demonstrated in the cremaster muscle of the mouse (Looft-Wilson *et al.*, 2004; Wolfle *et al.*, 2007). The effectiveness of electrical coupling in coordinating relaxation of SMCs was shown in feed arteries of the hamster retractor muscle, where injection of –0.8 nA into a single EC resulted in the conduction of hyperpolarization and vasodilation for distances exceeding 2 mm along vessels ~70 μm in diameter (Emerson and Segal, 2000a; 2001).

For intact vessels, electrical conduction along the endothelium can be influenced by coupling to surrounding SMCs and pericytes (Diep *et al.*, 2005; Zhang *et al.*, 2006; Zhang *et al.*, 2011) which in turn can be acted upon by perivascular nerves (Haug and Segal, 2005). *In vivo*, there are additional effects of luminal shear stress exerted by the flowing blood, vasoactive agents circulating in the bloodstream and the activity of surrounding parenchymal cells (Segal, 2005). Each of these stimuli obfuscates definitive resolution of intercellular signalling events that are intrinsic to the endothelium. For example, agents used to block GJCs, such as the glycyrrhetinic acid (GA) derivatives carbenoxolone (CBX) and 18β-glycyrrhetinic acid (βGA), may suppress endothelium-dependent responses of SMCs initiated through myoendothelial GJCs before their actions on EC : EC coupling become apparent. Such difference in susceptibility can be explained by the discrete nature of myoendothelial coupling, which contrasts with robust homocellular coupling within the endothelium (Emerson and Segal, 2000a; Sandow *et al.*, 2003). Thus, a vasomotor response of SMCs may be eliminated while electrical conduction along the endothelium remains intact. Moreover, GA derivatives purported to act on GJCs may have additional 'nonspecific' actions that could appear as the inhibition of myoendothelial coupling. For example, interfering with EC Ca^{2+} signalling or hyperpolarization could prevent SMC hyperpolarization independent of actions on myoendothelial GJCs (Tare *et al.*, 2002).

Despite the integral role of the endothelium in coordinating blood flow control, there is a dearth of information regarding either the nature or manipulation of intercellular coupling along the endothelium of resistance vessels in the absence of other cells, physical forces and chemical stimuli. Indeed, while EC: EC coupling has been demonstrated in resistance vessels from a variety of tissues and species (Bagher and Segal, 2011), electrical conduction along the native endothelium of blood vessels has not been evaluated in the absence of SMCs. Although electrical coupling between ECs has been assessed in cultured preparations (Larson *et al.*, 1983; Van Rijen *et al.*, 1997; Lidington *et al.*, 2000), the pronounced changes in cell morphology and phenotype together with the planar architecture of the two-dimensional monolayer in culture are unlike the morphology or physiology of ECs lining the resistance vasculature (Haas and Duling, 1997; Emerson and Segal, 2000b; Sandow *et al.*, 2003; Wolfle *et al.*, 2007). Thus, little is known of cell-to-cell coupling intrinsic to ECs that are integral to blood flow control. To provide such insight, the goal of this study was to define key properties of electrical conduction along intact EC tubes freshly isolated from resistance vessels of skeletal muscle (Socha *et al.*, 2011). For this purpose we dissected feed (superior epigastric) arteries from mouse abdominal skeletal muscle, thereby enabling unbranched segments up to ~3 mm long (width, ~60 μm) of intact endothelium following removal of SMCs. Using single and dual simultaneous intracellular microelectrodes, we tested two interrelated hypotheses: (i) Intercellular conduction of electrical signals through GJCs is manifest in freshly isolated EC tubes; and (ii) Inhibitors of GJCs have confounding effects on electrical and Ca^{2+} signalling. Our findings demonstrate that EC tubes are an effective conduit for electrical signals; however, confounding actions of GA derivatives prevent these agents from being used to resolve the role of GJCs from that of intermediate ($K_{Ca}3.1$, KCNN4)- and small ($K_{Ca}2.3$, KCNN3)-conductance Ca^{2+}-activated (IK_{Ca}/SK_{Ca}) K^+ channels in defining the nature of electrical conduction (channel nomenclature follows Alexander *et al.*, 2011).

Methods

Animal care and use

All animal care and experimental procedures were approved by the Animal Care and Use Committee of the University of Missouri and performed in accord with the National Research Council's *Guide for the Care and Use of Laboratory Animals* (8th ed., 2011). Mice were housed on a 12:12 h light-dark cycle at ~23°C with fresh water and food available *ad libitum*. Experiments were performed on C57BL/6 males bred at the University of Missouri (age, 3–6 months; n = 82). Each mouse was anaesthetized using pentobarbital sodium (60 $mg \cdot kg^{-1}$, intraperitoneal injection) and abdominal fur was removed by shaving. Following surgical procedures, the mouse was killed with an overdose of pentobarbital via cardiac injection.

Solutions

Physiological salt solution (PSS) was used to superfuse EC tubes [composition in mM: 140 NaCl, 5 KCl, 2 $CaCl_2$, 1 $MgCl_2$, 10 HEPES, 10 glucose, pH 7.4]. During vessel dissection and SMC dissociation to produce EC tubes, PSS con-

tained 0.1% bovine serum albumin (#10856, USB Corp., Cleveland, OH, USA). During dissection, $CaCl_2$ was absent and 0.01 mM sodium nitroprusside (SNP) was added to relax SMCs. During dissociation of SMCs, 0.1 mM $CaCl_2$ was added in lieu of SNP. Reagents were obtained from Sigma-Aldrich (St. Louis, MO, USA) unless otherwise indicated; corresponding catalogue numbers are shown in parentheses.

Surgery and microdissection

A ventral midline incision was made from the sternum to the pubis. While viewing through a stereo microscope (SMZ800, Nikon, Tokyo, Japan), fat and connective tissue superficial to the sternum was removed to expose the proximal ends of the abdominal muscle feed artery (AFA; defined anatomically as the superior epigastric artery) bilaterally. This artery was chosen based on our ability to obtain unbranched segments of sufficient length to determine length constant as a key measure of electrical conduction through GJCs. To maintain blood in the lumen and thereby facilitate visualization during dissection, each AFA was ligated along with its adjacent vein using 6-0 silk suture (Ethicon, Somerville, NJ, USA). Abdominal muscles were removed bilaterally and placed in chilled (4°C) dissection PSS. A muscle was pinned onto transparent silicone rubber (Sylgard 184, Dow Corning, Midland, MI, USA) and the AFA segment (length: ~2 cm) was dissected free from surrounding tissue. Residual blood was flushed from the vessel lumen by cannulating one end with a pipette made from heat-polished borosilicate glass capillaries (G150T-4, Warner Instruments, Hamden, CT, USA) with an outer diameter of 50–80 μm and connected to a column (height, 10 cm) of dissection PSS.

EC tube isolation and superfusion

The AFA was cut into segments (length, 1–3 mm) that were placed into PSS containing 0.62 mg·mL^{-1} papain (P4762), 1.0 mg·mL^{-1} dithioerythritol (D8255) and 1.5 mg·mL^{-1} collagenase (C8051), and incubated for 30 min at 34°C. Following partial digestion, the solution containing enzymes was replaced with dissociation PSS and AFA segments were transferred to a Petri dish (100 mm diameter × 15 mm high) and gently triturated to remove SMCs using borosilicate glass capillary tubes [1B100-4, World Precision Instruments (WPI), Sarasota, FL, USA] that were pulled (P-97, Sutter Instruments, Novato, CA, USA) and heat polished to a tip internal diameter of 80–120 μm. Following removal of SMCs (confirmed by visual inspection at 200× magnification), an EC tube was transferred to a tissue chamber (RC-27N, Warner Instruments) secured on an aluminium platform (length: 24 cm; width: 14.5 cm; thickness: 0.4 cm). The platform contained a micromanipulator (DT3-100, Siskiyou Corp., Grants Pass, OR, USA) at each end that held a blunted micropipette (heat polished, OD: 60–100 μm) to secure the tube against the bottom of the tissue chamber (24 × 50 mm coverslip).

The entire preparation was secured on an inverted microscope (Eclipse TS100, Nikon) mounted on a vibration-isolated table (Technical Manufacturing Corp., Peabody, MA, USA) and superfused at 4 mL·min^{-1} with PSS. Ejecting blue dye from micropipettes confirmed that superfusion flow was laminar along the axis of EC tubes. The temperature of the chamber was regulated using an inline heater (SH-27B, Warner Instruments) and heating platform (PH6, Warner Instruments) coupled to a temperature controller (TC-344B, Warner Instruments). Temperature was increased over 30 min to 32°C where intact preparations were stable for over 3 h (Socha *et al.*, 2011). Pharmacological agents were added to the superfusion solution, thereby exposing the entire EC tube to the agent.

Intracellular recording

Membrane potential (V_m) in EC tubes was recorded with an Axoclamp amplifier (2B, Molecular Devices, Sunnyvale, CA, USA) using microelectrodes pulled (P-97, Sutter Instruments) from glass capillary tubes (GC100F-10, Warner Instruments) and backfilled with 2 M KCl (tip resistance: ~150 MΩ). For experiments in testing dye coupling, microelectrodes were backfilled with 0.1% propidium iodide (mass, 668 Da) dissolved in 2 M KCl. An Ag/AgCl pellet placed in the effluent PSS served as a reference electrode. The output of the amplifier was connected to a data acquisition system (Digidata 1322A, Molecular Devices) and an audible baseline monitor (ABM-3, WPI). For dual simultaneous intracellular recordings (Emerson and Segal, 2000a), a second amplifier (IE-210, Warner Instruments) was integrated into the data acquisition system. Current (±0.1–3 nA, 2 s pulse duration) was delivered using the Axoclamp electrometer driven by a function generator (CFG253, Tektronix, Beaverton, OR, USA).

For current injection, an EC was penetrated at 'Site 1' located ~150 μm from where the EC tube was secured at one end. For simultaneous recording of V_m, a second EC was impaled at 'Site 2' located 50–2000 μm from Site 1 along the midline of the EC tube. The length of individual ECs in this preparation is ~35 μm (Socha *et al.*, 2011). Thus, a minimum separation distance of 50 μm between microelectrodes ensured that Sites 1 and 2 were always in separate cells. For evaluating the effects of CBX and βGA on electrical conduction, separation distance between microelectrodes was standardized at 500 μm, which corresponds to the distance of ~15 ECs placed end to end (Socha *et al.*, 2011).

Successful impalements were indicated by sharp negative deflection of V_m, stable V_m for >1 min, hyperpolarization (≥20 mV) to either 3 μM ACh (indirect IK_{Ca}/SK_{Ca} channel agonist) or 1 μM NS309 (direct IK_{Ca}/SK_{Ca} channel activator, Tocris, Bristol, UK), recovery to resting V_m after ACh or NS309 washout and prompt return to ~0 mV upon withdrawal from the cell. Correspondence between current injection at Site 1 and V_m responses at Site 2 provided an additional indicator of successful simultaneous intracellular current injection and V_m recording. Data were acquired at 1000 Hz on a Dell Personal Computer using Axoscope 10.1 software (Molecular Devices). Following propidium iodide dye microinjection, using a standard filter set for rhodamine dye with illumination from a 50 W Hg lamp, fluorescence images were acquired using a 40× objective (Nikon Fluor40; numerical aperture, 0.75) and focused onto a cooled charge-coupled device camera (MicroFire, Optronics, Goleta, CA, USA).

Calcium photometry

Ca^{2+} photometry in EC tubes was performed using an IonOptix system (Milford, MA, USA) as recently described (Socha *et al.*, 2011). Briefly, an EC tube was equilibrated for ~15 min

in the recording chamber during superfusion with PSS at room temperature. Fura-2 AM dye (F14185, Invitrogen, Carlsbad, CA, USA) dissolved in DMSO was diluted to 10 μM in PSS (final DMSO concentration <0.5%). The EC tube was incubated for 30 min without flow then superfused with PSS for 30 min to wash out excess dye and allow Fura-2 within cells to de-esterify. Temperature was raised to 32°C during a period of 30 min and maintained at 32°C thereafter (Socha *et al.*, 2011). Using a 20× objective (Nikon Fluor20, NA 0.75), Fura-2 dye was excited alternately (250 Hz) at 340 and 380 nm while fluorescence emission was collected at 510 nm and expressed as a F_{340}/F_{380} ratio. Autofluorescence values at 510 nm during excitation at 340 and 380 nm were recorded prior to dye loading and subtracted from respective recordings.

Pharmacology

ACh chloride and NS309 were used to evoke hyperpolarization of EC tubes via indirect and direct activation of IK_{Ca}/SK_{Ca} channels respectively (Busse *et al.*, 2002; Strobaek *et al.*, 2004). Responses to ACh and NS309 were studied through a similar range of concentrations by addition to the superfusion solution. Once a stable peak response V_m was recorded for a given agonist concentration, washout with control PSS for several min restored baseline conditions and the next concentration was added. In time controls for repeated exposures to 3 μM ACh, hyperpolarization remained similar (ΔV_m ~ −35 mV) for ~20 exposures over 3 h (n = 3). CBX and βGA were used to test for inhibition of electrical conduction and dye coupling through GJCs (Yamamoto *et al.*, 1998; Tare *et al.*, 2002; Zhang *et al.*, 2006; Dora *et al.*, 2008; Kansui *et al.*, 2008). Compounds were prepared at a stock concentration of 50 mM and diluted to final concentrations in PSS; pH 7.4 was maintained throughout experiments. NS309 and βGA were dissolved in DMSO before dilution (final DMSO concentration ≤ 1%). Vehicle controls (≤2% DMSO in PSS) had no effect on V_m or electrical coupling (n = 3).

Data analysis

One EC tube was studied per mouse. For intracellular recordings, analyses included: (i) change in V_m (ΔV_m) = peak response V_m – resting baseline V_m; (ii) conduction amplitude = ΔV_m at Site 2/current injected at Site 1; and (iii) length constant (λ) = distance over which the electrical signal decayed to 37% (1/e) of the initial value. The initial value was taken as ΔV_m measured at 50 μm separation distance to ensure that both microelectrodes were not in the same EC while recording as close to the signal origin as possible. Linear regression (ΔV_m at Site 2 vs. current injection at Site 1), curve fitting (concentration responses for pEC_{50} determinations) and estimates of λ were performed using GraphPad Prism (GraphPad Software, Inc., La Jolla, CA, USA). Calcium photometry data are presented as F_{340}/F_{380} ratios. Changes in baseline ratio were calculated as the F_{340}/F_{380} ratio following 10 min equilibration with each [CBX] or [βGA] minus the initial baseline ratio under control conditions. The change in F_{340}/F_{380} ratio in response to ACh was calculated as the peak F_{340}/F_{380} ratio minus the baseline preceding stimulation with ACh. Statistical analyses included repeated measures analysis of variance with Tukey or Bonferroni *post hoc* comparisons and paired *t*-tests performed using GraphPad Prism. Differences between groups were accepted as statistically significant with $P < 0.05$. Summary data are presented as means ± SE.

Results

Freshly dissociated EC tubes approximated the dimensions of microvessels, being ~60 μm wide and up to 3 mm long. Mechanical stability of EC tubes enabled continuous intracellular recordings of V_m lasting up to 4 h. Thus, concentration–response curves and the effect of experimental interventions on V_m were typically recorded from the same impalements.

Hyperpolarization of EC tubes to indirect and direct activation of IK_{Ca}/SK_{Ca} channels

During continuous recording, EC tubes readily hyperpolarized to ACh and to NS309 (Figure 1A). From a resting V_m of −26 ± 5 mV, there was a clear concentration-dependent increase in hyperpolarization with NS309, resulting in a maximal ΔV_m of −52 ± 1 mV at 10–30 μM with a pEC_{50} of 6.40 ± 0.06 (Figure 1B, n = 5). From a resting V_m of −27 ± 2 mV, hyperpolarization also increased concentration-dependently with ACh, resulting in a maximal ΔV_m of −37 ± 5 mV at 3 μM ACh with a pEC_{50} of 6.88 ± 0.09 (Figure 1C, n = 9). As an index of Ca^{2+} signalling underlying hyperpolarization, peak $[Ca^{2+}]_i$ in Fura-2 loaded EC tubes reached a maximum at 1 μM ACh with a pEC_{50} of 7.34 ± 0.04 (Figure 1D, n = 5). As hyperpolarization to 1 μM NS309 (−37 ± 2 mV) was not different from that in response to 3 μM ACh, these respective concentrations were used as standard stimuli in subsequent experiments.

Electrical conduction during current microinjection

Dual simultaneous intracellular recording confirmed similar resting V_m at two sites separated by 500 μm (V_m1 = −25 ± 1, V_m2 = −25 ± 1 mV, n = 15). Electrical coupling along EC tubes was tested by injecting current (±0.1–3 nA, 2 s pulses) during V_m recording at Site 1 while measuring V_m at Site 2 with a defined distance between microelectrodes (e.g. 500 μm in Figure 2A). At a given separation distance, conduction amplitude increased linearly with current injected of either polarity (Figure 2B). As separation distance increased, the relationship between ΔV_m2 and current injected at Site 1 decreased proportionally (Figure 2B; note reduced slope at 1500 μm vs. 500 μm). Given the linear (i.e. ohmic) response of ΔV_m2 to current injected at each separation distance ($R^2 \geq 0.99$; Figure 2B), conduction amplitude at each distance was routinely estimated from ΔV_m2 recorded during −1 nA current. From an initial value of 11.4 ± 0.4 mV·nA^{-1} at 50 μm separation, conduction amplitude decayed monoexponentially with distance, resulting in λ = 1360 ± 100 μm (Figure 2C, n = 8).

Inhibition of electrical conduction with GA derivatives

Recorded 500 μm from Site 1, V_m responses at Site 2 with ±0.1–3 nA current injection under control conditions are

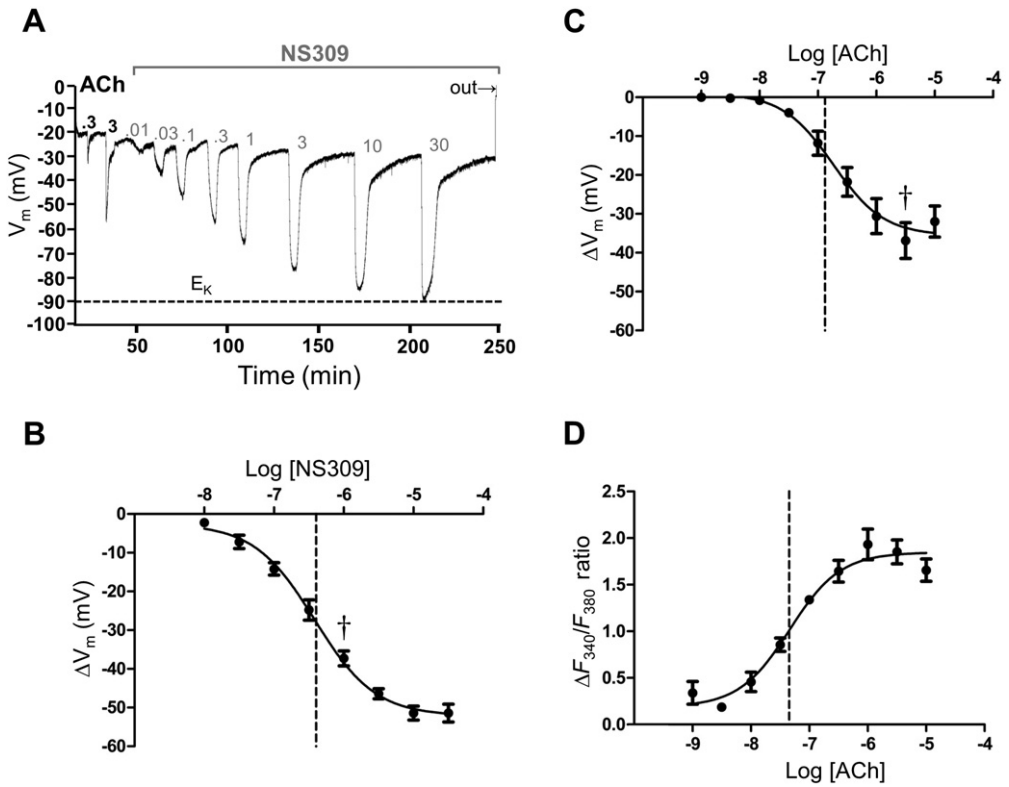

Figure 1

Membrane potential and Ca^{2+} responses in EC tubes. (A) Continuous 4 h record of V_m from one cell within an EC tube illustrating hyperpolarization to ACh (0.3 and 3 μM) followed by NS309 (0.01–30 μM) with washout following each peak hyperpolarization. The value for E_K = –90 mV was calculated with $[K^+]_o$ = 5 and $[K^+]_i$ = 145 mM. (B) Peak hyperpolarization for indicated concentrations of NS309 (n = 5); ΔV_m (mV) = resting V_m – peak response V_m. (C) Peak hyperpolarization for indicated concentrations of ACh (n = 9). ΔV_m calculated as in B. (D) Peak $[Ca^{2+}]_i$ responses for indicated concentrations of ACh (n = 5) using Fura-2 dye. $\Delta F_{340}/F_{380}$ = peak response F_{340}/F_{380} – resting F_{340}/F_{380}. Respective pEC_{50}s indicated by vertical broken lines are: (B) 6.40 ± 0.06; (C) 6.88 ± 0.09; (D) 7.34 ± 0.04. †ΔV_m for 1 μM NS309 ≈ ΔV_m for 3 μM ACh. Summary data are means ± SE.

shown in Figure 3A. Representative records are shown for treatments with CBX (Figure 3B, C) and for βGA (Figure 3E–G) with summary data for respective agents in Figure 3D, H. For CBX, 30 μM did not alter V_m responses to ±1 nA (Figure 3B) while 100 μM inhibited responses within 5 min (Figure 3C). With βGA, responses of V_m at Site 2 were maintained during exposure to 10 μM (Figure 3E) but were inhibited within 10 min by 30 μM (Figure 3F) and within 5 min by 40 μM (Figure 3G). Summary data indicate significant ($P < 0.05$) inhibition of electrical conduction by 100 μM CBX (Figure 3D, n = 4) and with βGA ≥ 30 μM (Figure 3H, n = 5). Conduction amplitude recovered following ~20 min washout of either GA derivative (to 8 ± 1 mV·nA^{-1}; n = 6).

Inhibition of dye transfer with GA derivatives

As an independent test of intercellular coupling through GJCs, an EC was penetrated with a microelectrode containing propidium iodide (0.1%). After 30 min, fluorescence in multiple neighbouring ECs indicated robust dye transfer (Figure 4A, D). When either 100 μM CBX or 40 μM βGA was applied for ~5 min before an EC was impaled, dye was confined to the impaled cell (n = 6; Figure 4B, E) when examined after 30 min of recording. In half of these experiments, we tested for reversibility and dye transfer was restored after 20 min washout of either CBX (n = 2; Figure 4C) or βGA (n = 1; Figure 4F). Treatment with lower concentrations of CBX (30 μM) or βGA (10 μM) for the same duration partially inhibited dye transfer, with reversibility apparent upon washout (Supporting Information Figure S1).

Inhibition of hyperpolarization to ACh with GA derivatives

These experiments were performed using single microelectrode recordings to evaluate concentration-dependent effects of CBX and βGA on EC hyperpolarization in the complete absence of SMCs. To indirectly activate IK_{Ca}/SK_{Ca} channels, ACh (3 μM) was applied for ~2 min under control conditions and during increasing concentrations of CBX or βGA (3–100 μM). Each treatment began 5 min before exposure to ACh. Hyperpolarization to ACh was attenuated significantly by 30 μM CBX and nearly eliminated by 100 μM CBX (Figure 5A–D). Greater potency and efficacy were apparent with βGA, which attenuated hyperpolarization at 10 μM and abolished hyperpolarization at 30–100 μM (Figure 5E–H).

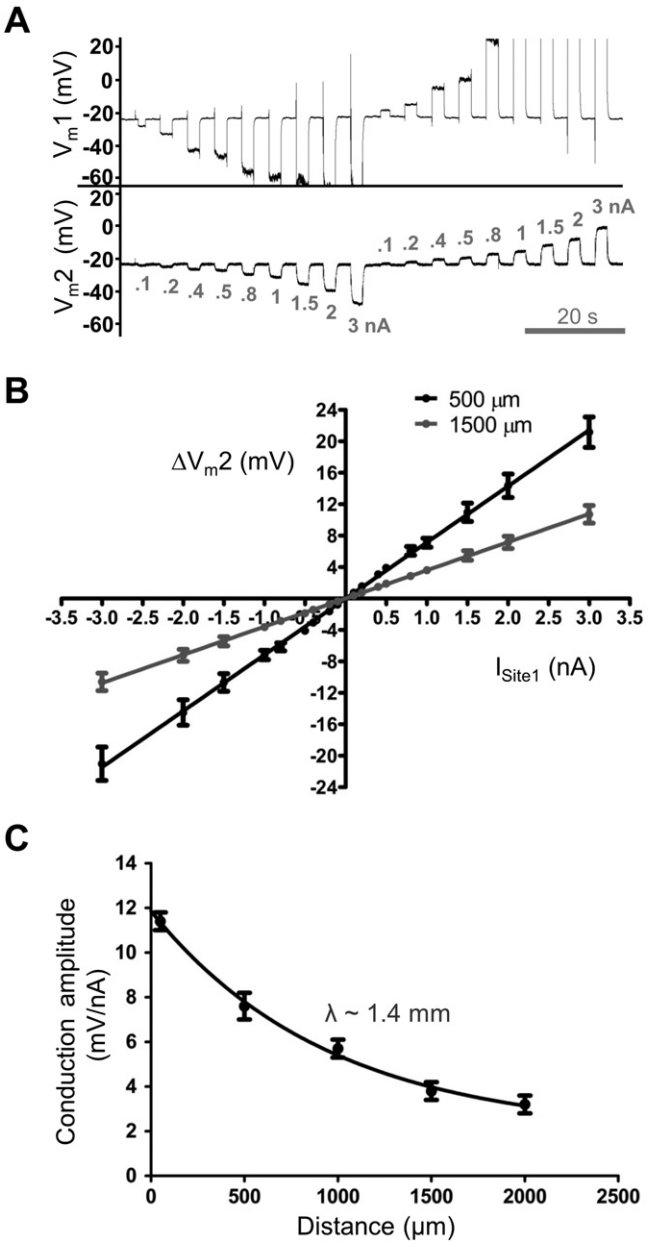

Figure 2

Electrical conduction determining length constant. (A) Representative dual simultaneous intracellular recording illustrating V_m traces at Site 1 (V_m1) and Site 2 (V_m2) separated by 500 µm. Current pulses (±0.1–3 nA, 2 s each) were injected at Site 1 while V_m was recorded at Sites 1 and 2. (B) Plot of summary data (means ± SE) for current injected into Site 1 versus ΔV_m at Site 2. Black line: recordings at 500 µm separation (n = 15); slope by linear regression (R^2 = 1) represents conduction amplitude = 7.0 ± 0.7 mV·nA^{-1} (n = 15). For single-point reference, conduction amplitude calculated for –1 nA current = 7.2 ± 0.6 mV·nA^{-1}. Grey line: recordings at 1500 µm separation (n = 8). (C) Conduction amplitude (ΔV_m2 in response to –1 nA current injection at Site 1) with increasing separation distance between Sites 1 and 2 (50 µm: 11.4 ± 0.4; 500 µm: 7.6 ± 0.6; 1000 µm: 5.7 ± 0.4; 1500 µm: 3.8 ± 0.4; 2000 µm: 3.2 ± 0.4 mV·nA^{-1}). Length constant (λ) = 1360 ± 100 µm calculated from monoexponential fit (R^2 = 0.99) to summary data (n = 8 for 50–1500 µm; n = 4 at 2000 µm).

Inhibition of hyperpolarization to ACh or NS309 upon loss of electrical conduction

These experiments were performed with 500 µm separation distance between microelectrodes to determine whether loss of electrical conduction during exposure to GA derivatives coincided with loss of hyperpolarization initiated by activation of IK_{Ca}/SK_{Ca} channels. Before βGA or CBX treatments, changes in V_m2 were simultaneous with current injections into Site 1 (Figure 6A, D respectively). Application of either 40 µM βGA (Figure 6A) or 100 µM CBX (Figure 6D) hyperpolarized ECs by 15–20 mV within 10–15 s. These changes in V_m were greatest after ~1 min (ΔV_m: βGA: –19 ± 2 mV, n = 9; CBX: –14 ± 3 mV, n = 6) and persisted 2–3 min. After 4–6 min of continuous exposure, V_m recovered to approximate the initial (control) value. At this time, electrical conduction was abolished by βGA (Figure 6A) and by CBX (Figure 6D) with only residual capacitance spikes remaining. Coincident with loss of electrical coupling, the input resistance (calculated as ΔV_m/nA current at Site 1) increased from 41 ± 5 to 154 ± 11 MΩ (P < 0.01; n = 15). Continued exposure to either GA derivative beyond 6 min consistently depolarized V_m to –8 ± 1 mV (n = 20; Figure 6C, F).

Under control conditions, application of 3 µM ACh (Figure 6B) or 1 µM NS309 (Figure 6E) hyperpolarized ECs by a similar amount over 1–2 min [ΔV_m for ACh: –39 ± 4 mV (n = 8); ΔV_m for NS309: –39 ± 2 (n = 12)]. Whereas hyperpolarization waned during prolonged exposure to ACh (Figure 6B), hyperpolarization to NS309 persisted throughout the duration of exposure (Figure 6E). Upon block of electrical conduction by either GA derivative, ACh (Figure 6C) or NS309 (Figure 6F) no longer evoked hyperpolarization (n = 8 and n = 12 respectively). Hyperpolarization to ACh or NS309 recovered (ΔV_m = –34 ± 3 mV; n = 7) following ~20 min washout of either CBX or βGA.

Effects of GA derivatives on Ca^{2+} responses

ACh (3 µM) was applied under control conditions and again during exposure (10 min each) to CBX or βGA (10, 30 or 100 µM). Following the final treatment, the preparation was superfused for 20 min with control PSS to obtain a final (recovery) response to ACh. Time controls verified that $[Ca^{2+}]_i$ responses to identical repeated exposures to 3 µM ACh in control PSS (with 10 min washout in between) were reproducible for at least 90 min (n = 2).

Representative $[Ca^{2+}]_i$ responses are shown in Figure 7A (CBX) and Figure 7D (βGA). The baseline F_{340}/F_{380} ratio increased progressively with the concentration of either GA derivative (n = 3 each) and was significantly greater (P < 0.05) than control at 30 and 100 µM (Figure 7B, E). The elevated baseline F_{340}/F_{380} ratio returned towards control following washout of either agent (Figure 7A, B, D, E). With CBX, the overall amplitude of $[Ca^{2+}]_i$ responses to ACh was not significantly different from control (Figure 7C). However, recovery $[Ca^{2+}]_i$ responses were significantly enhanced (P < 0.05) following washout (Figure 7C). With βGA, $[Ca^{2+}]_i$ responses to ACh were abolished using 100 µM (Figure 7D, F), suggesting that greater lipophilicity of βGA may influence internal Ca^{2+} stores. In contrast to treatment with CBX, washout of βGA did not enhance $[Ca^{2+}]_i$ responses during recovery (Figure 7F).

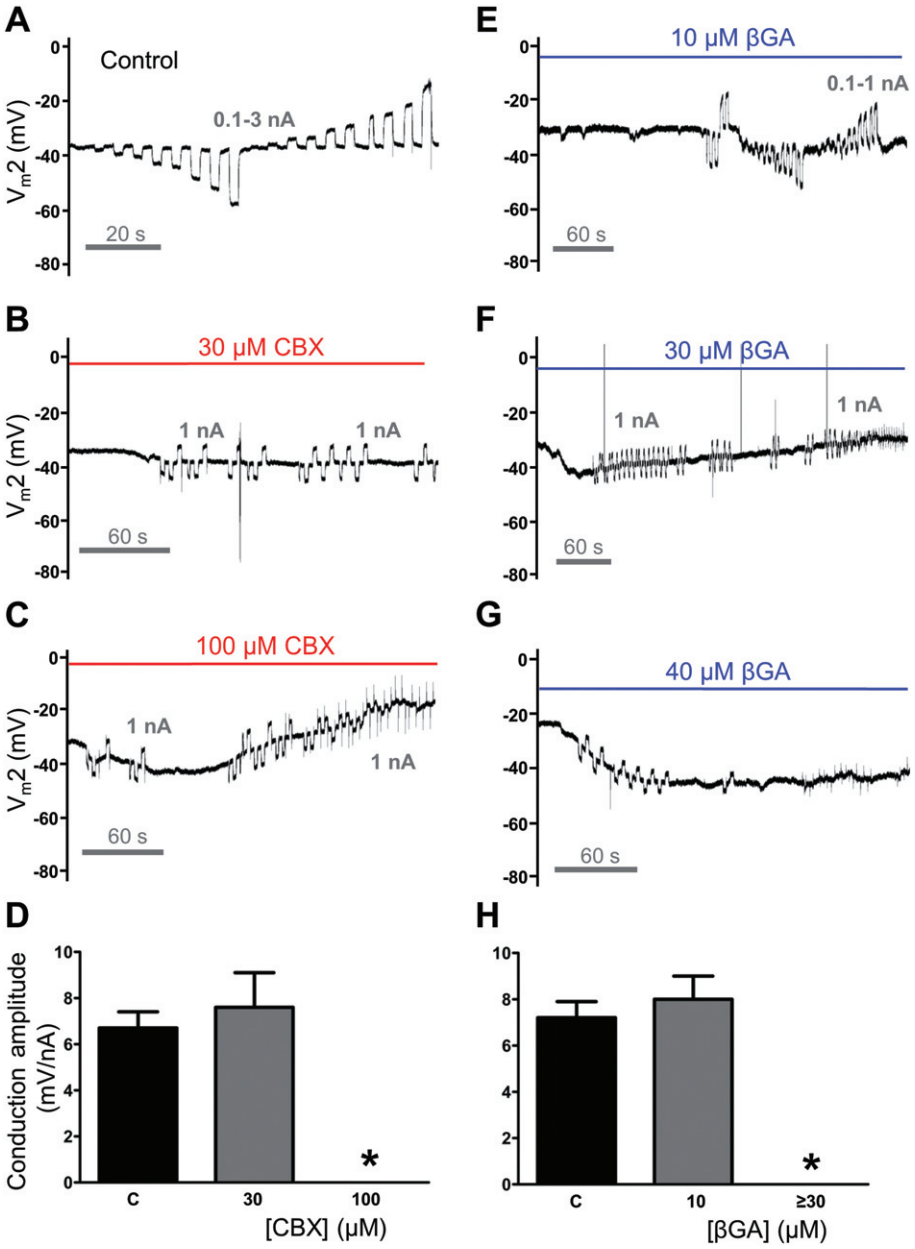

Figure 3

Inhibition of electrical conduction by CBX and βGA. Representative responses of V_m at Site 2 recorded 500 μm from current injection at Site 1 under control conditions and during exposure to GA derivatives. Indicated treatments began at the time of the recordings illustrated. (A) Control responses to ±0.1–3 nA. (B) During 30 μM CBX, V_m responses to ±1 nA were maintained with no effect on baseline V_m. (C) During exposure to 100 μM CBX, V_m initially hyperpolarized and then depolarized; after ~5 min, V_m responses to ±1 nA were inhibited such that only residual capacitance spikes remained. (D) Summary data (means ± SE; $n = 4$) for experiments illustrated in A–C. Responses during 30 μM CBX were not different from control (**C**). Electrical coupling was abolished during 100 μM CBX. *Significantly different from control, $P < 0.05$. (E) Responses to ±0.1–3 nA were maintained during 10 μM βGA. (F) During 30 μM βGA, V_m responses to ±1 nA were inhibited within ~10 min. (G) During 40 μM βGA, V_m responses to ±1 nA were inhibited within ~5 min. (H) Summary data (means ± SE; $n = 5$) for experiments in E–G. Responses during 10 μM βGA were not different from control (**C**). Electrical coupling was abolished with ≥30 μM βGA. *Significantly different from control, $P < 0.05$.

Discussion and conclusions

This study investigated the electrophysiological properties of intact EC tubes freshly isolated from feed arteries of abdominal skeletal muscle of the C57BL/6 mouse. Current injected into a single EC produced robust proportional changes in V_m along the entire tube for depolarizing and hyperpolarizing signals. Further, propidium iodide dye injected into one EC spread radially into neighbouring ECs. These findings illustrate the viability of EC tubes as a model to investigate intercellular electrical conduction and support the hypothesis that individual cells within EC tubes are effectively coupled to each

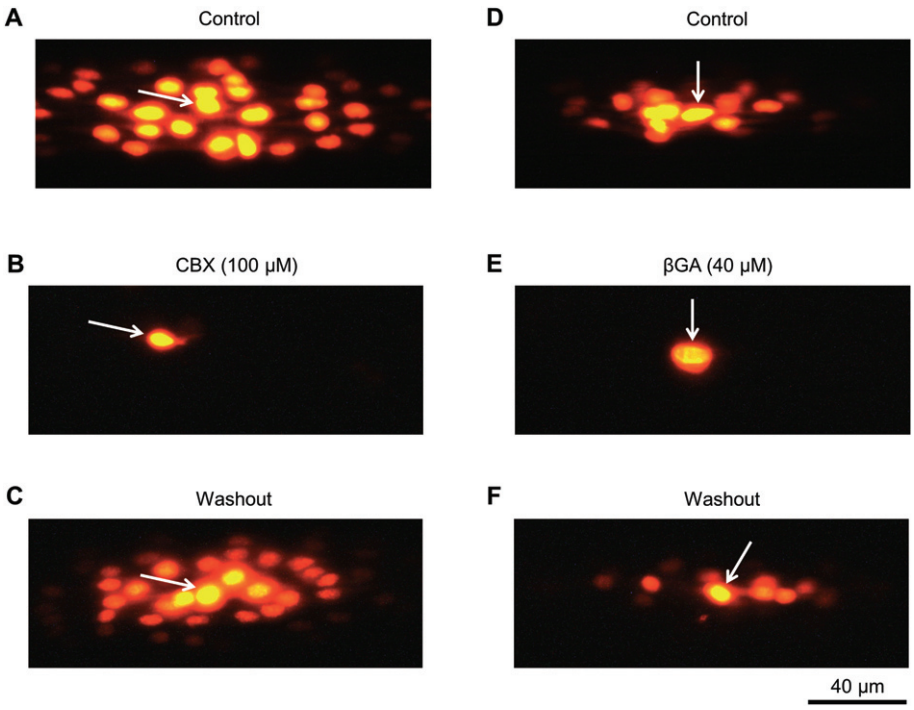

Figure 4

Reversible inhibition of dye transfer by CBX and βGA. Representative images following propidium iodide microinjection (into cell indicated by arrow). (A) Propidium iodide dye (0.1% in 2 M KCl) was microinjected under control conditions during intracellular recording for 30 min. Note robust dye transfer to surrounding cells. (B) As described in A at a separate site of the same EC tube after 5 min exposure to 100 μM CBX that was maintained during 30 min intracellular recording. Note absence of dye transfer. (C) As described in A at a separate site of the same EC tube following 20 min washout of 100 μM CBX with PSS. Note restoration of dye transfer. (D) As described in A. (E) As in B using 40 μM βGA instead of CBX. Note absence of dye transfer. (F) As described in C following 20 min washout of 40 μM βGA with PSS.

other through GJCs. Further, we showed that inhibition of GJCs with CBX or βGA also inhibited EC hyperpolarization in response to either indirect (ACh) or direct (NS309) activation of IK_{Ca}/SK_{Ca} channels. Importantly, the loss of hyperpolarization coincided with the inhibition of electrical conduction and dye transfer. Thus, neither of these GA derivatives resolve the role of GJCs from that of IK_{Ca}/SK_{Ca} channel activation in defining electrical conduction along the endothelium.

V_m of EC tubes

Following isolation and equilibration, resting V_m in EC tubes averaged –25 mV. Mathematical modelling of rat mesenteric arteries predicts that, in the absence of electrical coupling to SMCs, the V_m of ECs is –24.9 mV (Kapela *et al.*, 2009). In preparations of rat mesenteric arteries exhibiting myoendothelial coupling, V_m of ECs was –54 mV (and –57 mV in SMCs), while in the femoral artery (devoid of myoendothelial coupling) V_m of ECs averaged –26 mV (with –58 mV in SMCs) (Sandow *et al.*, 2002). Thus, the less negative V_m recorded here in EC tubes compared with ECs of intact arteries may be explained by loss of input (via myoendothelial coupling) from voltage-gated K^+ (K_V) channels in SMCs (Jackson, 2005). Under such conditions, the V_m of ECs may reflect membrane conductance to non-selective cation channels (Nilius and Droogmans, 2001; Jackson, 2005; Kapela *et al.*, 2009). For the present study, an important feature is that EC tubes readily hyperpolarize upon exposure to ACh or to NS309 as well as during current microinjection (Figures 1 and 2). At the same time, a limitation of this preparation is that it cannot be used to evaluate the role of SMCs or of myoendothelial coupling in modulating the functional properties of the endothelium.

Hyperpolarization and vasodilation through activation of IK_{Ca}/SK_{Ca} channels

ACh is a G-protein-coupled, endothelium-dependent vasodilator that liberates inositol trisphosphate (IP_3) and triggers internal release of Ca^{2+} from the endoplasmic reticulum, 'indirectly' activating IK_{Ca}/SK_{Ca} channels to initiate hyperpolarization (Busse *et al.*, 2002). In support of ACh as a stimulus to investigate the dependence of indirect activation of IK_{Ca}/SK_{Ca} channels on a rise in $[Ca^{2+}]_i$ in EC tubes, the pEC_{50} value we determined for $[Ca^{2+}]_i$ responses (7.34; Figure 1D) was lower than for membrane hyperpolarization (6.88; Figure 1C). The synthetic compound NS309 is a potent direct activator of IK_{Ca}/SK_{Ca} channels with negligible effect on other ion channels (Strobaek *et al.*, 2004). At concentrations ≤10 μM, NS309 evokes hyperpolarization without changing EC $[Ca^{2+}]_i$ (Sheng *et al.*, 2009; Brondum *et al.*, 2010; Dalsgaard *et al.*, 2010). Despite having a pEC_{50} for hyperopolarization (6.40, Figure 1B) of higher concentration than determined for ACh (6.88, Figure 1C), NS309 produced greater peak hyperpolarization (ΔV_m, –50 to –60 mV vs. –30 to –40 mV; Figure 1A–C). Further, peak hyperpolarization to ACh was transient (Figure 6B) while that to NS309 was sustained (Figure 6E).

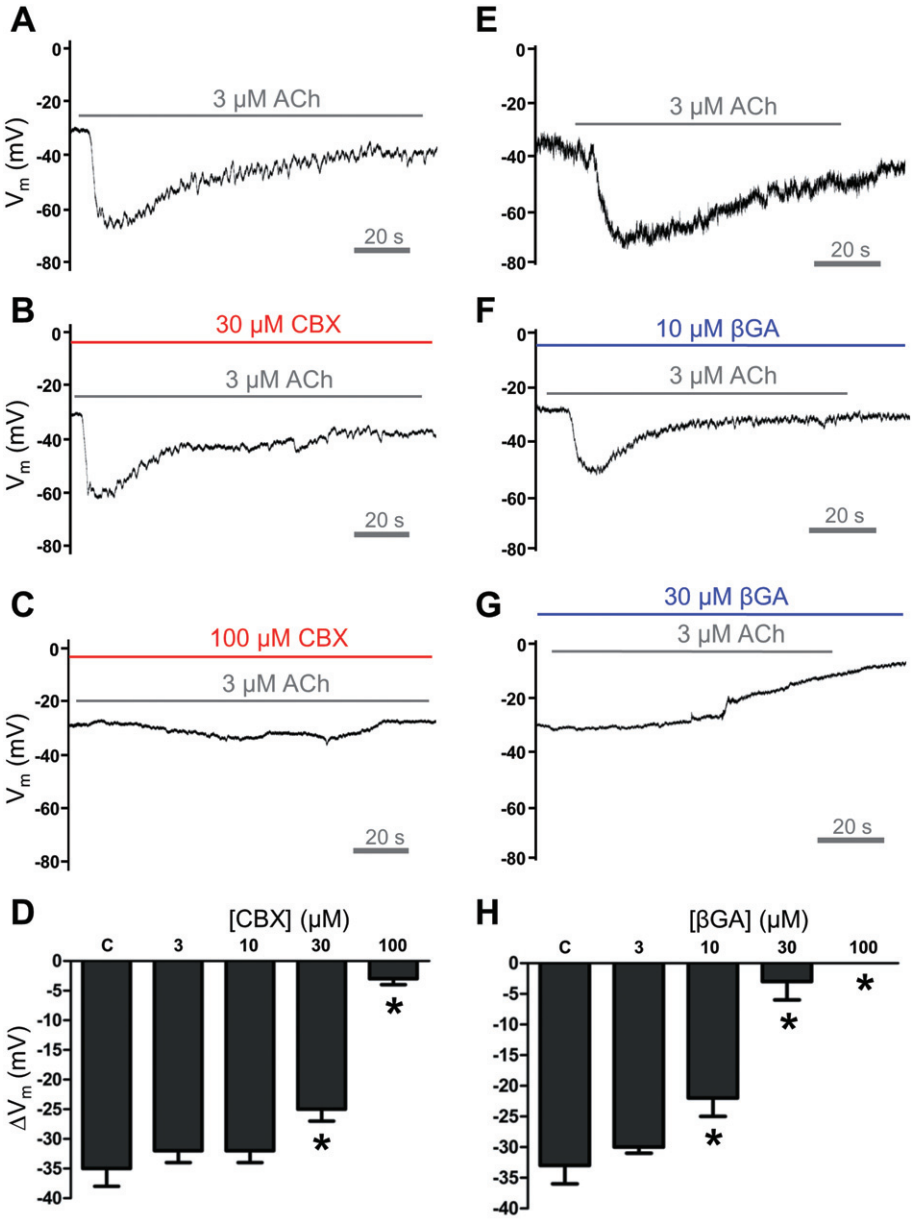

Figure 5

Inhibition of hyperpolarization to ACh by CBX and βGA. Representative responses of V_m to ACh under control conditions and during exposure to GA derivatives. Treatment with each respective GA derivative was initiated 5 min prior to records shown. (A) Control recording of hyperpolarization to ACh. (B) Attenuated hyperpolarization to ACh during exposure to 30 μM CBX. (C) Inhibition of hyperpolarization to ACh during exposure to 100 μM CBX. (D) Summary data for effect of [CBX] on hyperpolarization to ACh (n = 7). *Significantly different from control (**C**), $P < 0.05$. (E) Control recording of hyperpolarization to ACh. (F) Attenuated hyperpolarization to ACh during 10 μM βGA. (G) Inhibition of hyperpolarization to ACh during spontaneous depolarization to 30 μM βGA. (H) Summary data for effect of [βGA] on hyperpolarization to ACh (n = 3). *Significantly different from control (**C**), $P < 0.05$. Note transient nature of hyperpolarization during periods of ACh stimulation in A, B, E and F.

Such behaviour supports the conclusion that IK_{Ca}/SK_{Ca} channels did not inactivate during NS309 exposure, thereby enabling peak hyperpolarization with NS309 to approximate E_K (Figure 1A). Indeed, the dynamic range of V_m in EC tubes (i.e. from –25 mV at rest to –90 mV at E_K) revealed through activation of IK_{Ca}/SK_{Ca} channels emphasizes the integral role of these ion channels in governing V_m of the endothelium. The ability of ACh to effect hyperpolarization (and vasodilation) through indirect activation of IK_{Ca}/SK_{Ca} channels (Busse *et al.*, 2002) reinforces the use of this agonist as a common tool for studying endothelium-dependent hyperpolarization (Bagher and Segal, 2011; Garland *et al.*, 2011).

Electrical conduction along EC tubes

Dual intracellular microelectrodes enable the injection of current into one cell while measuring V_m in another cell at

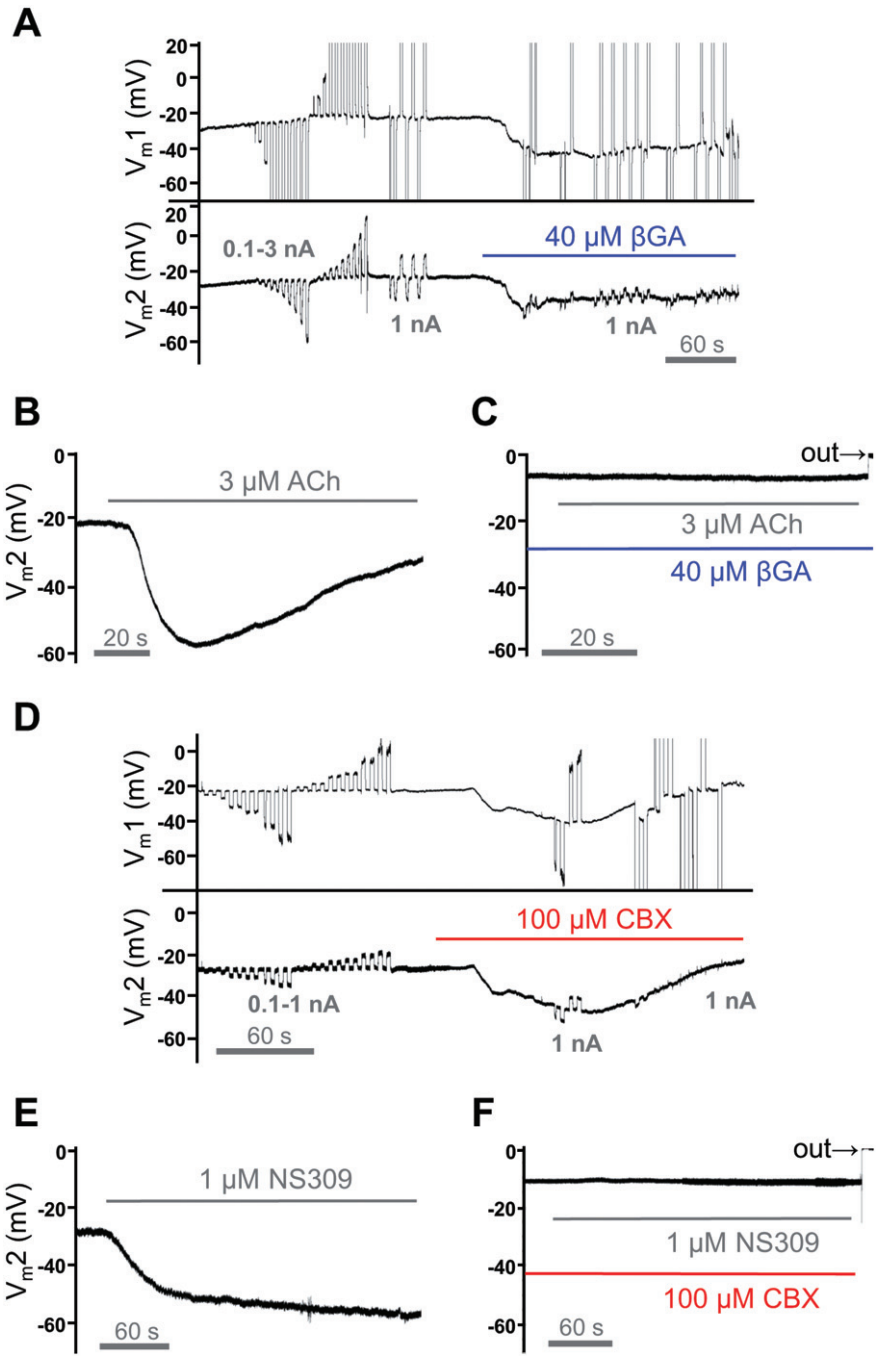

Figure 6

Inhibition of hyperpolarization to ACh or NS309 upon loss of electrical conduction. (A) Control V_m responses at Site 1 (V_m1) and Site 2 (V_m2) to ±0.1–3 nA injected at Site 1 followed by treatment with 40 μM βGA. Note ~20 mV hyperpolarization during βGA followed by loss of V_m2 responses coincident with increased V_m1. The latter effect reflects greater input resistance during current injection. (B) Control response to ACh at Site 2 before current injections; note transient hyperpolarization during continuous exposure to ACh. (C) Recording at Site 2 in the presence of βGA after loss of electrical conduction in A. After 6–7 min of exposure to βGA, note depolarization to < –10 mV and lack of hyperpolarization to ACh; recording is representative of $n = 5$ with 40 μM βGA and $n = 3$ with 100 μM CBX. (D) Control V_m responses at Site1 (V_m1) and Site 2 (V_m2) to ±0.1–1 nA injected at Site 1 followed by treatment with 100 μM CBX. During CBX treatment, note transient ~20 mV hyperpolarization followed by loss of V_m2 responses (small residual capacitance spikes remain). Coincident increase of V_m1 responses reflects greater input resistance during current injection. (E) Response to NS309 at Site 2 before current injections. Note sustained hyperpolarization during exposure to NS309 versus transient response to ACh in B. Hyperpolarization to NS309 reversed within 10 min after washout (not shown). (F) Recording at Site 2 in the presence of CBX after loss of electrical conduction in A. After 6–7 min of exposure to CBX, note depolarization to –10 mV and lack of hyperpolarization to NS309; recording is representative of $n = 4$ with 100 μM CBX and $n = 8$ with 40 μM βGA. Reference to 'out' on V_m recordings in C and F illustrates withdrawal of microelectrode from cell, confirming stability of intracellular recording throughout these experiments.

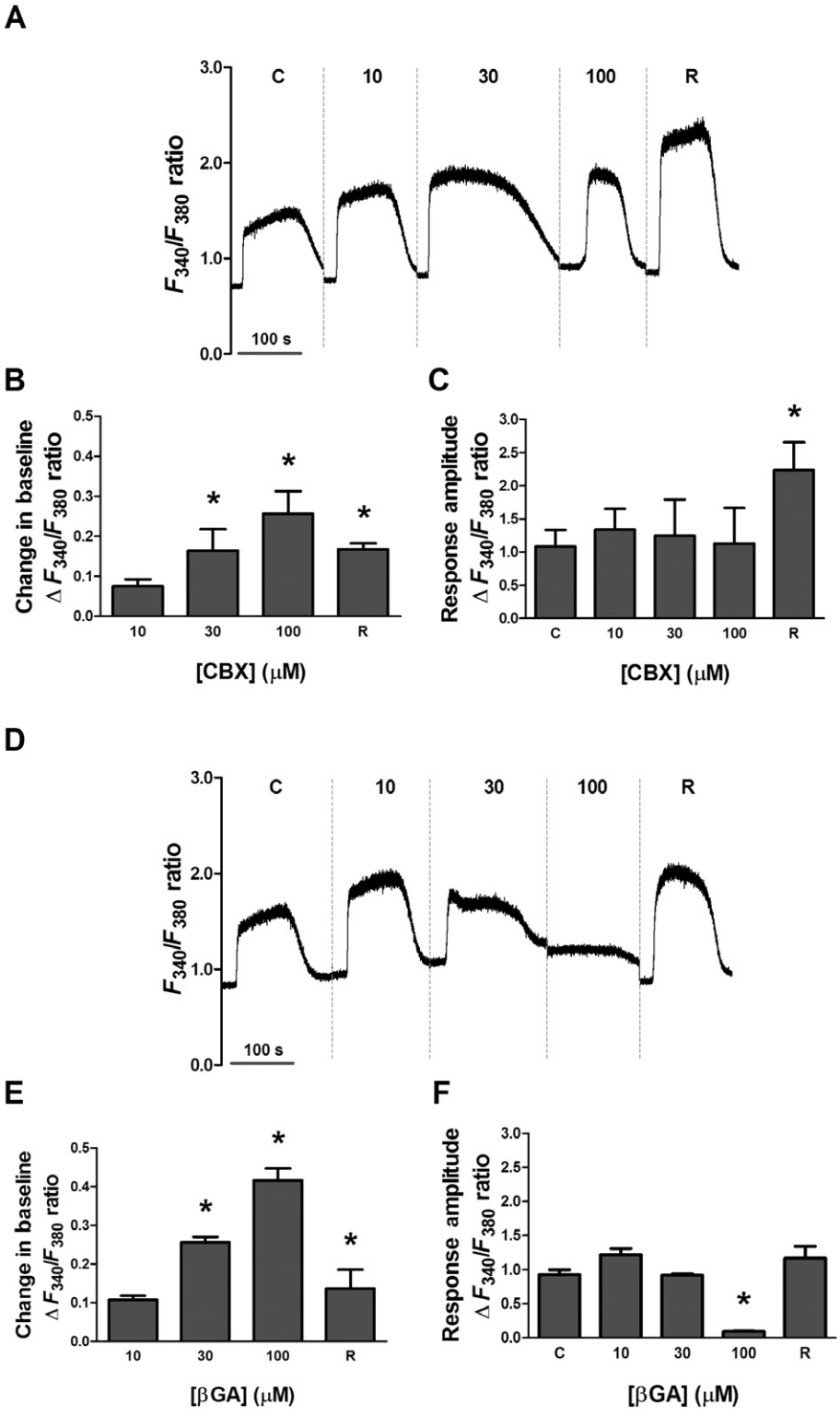

Figure 7

Effect of GA derivatives on $[Ca^{2+}]_i$ responses to ACh. (A) Representative recording of EC $[Ca^{2+}]_i$ responses to 1 min superfusion of 3 μM ACh under control (**C**) conditions, following 10 min exposure to 10, 30 or 100 μM CBX, and following 20 min recovery (R) during washout of CBX. Vertical lines denote 10 min breaks in recording during superfusion with CBX in PSS at respective concentrations before ACh stimulation. (B) Summary data ($n = 3$) for the change in baseline F_{340}/F_{380} ratio from resting control following 10 min superfusion with 10, 30 or 100 μM CBX and during recovery (R) following 20 min washout. (C) Summary data ($n = 3$) for response amplitude [= (maximal F_{340}/F_{380} ratio during 1 min ACh) – (preceding baseline F_{340}/F_{380} ratio)] under control conditions (**C**) and after 10 min exposure to respective [CBX]. (D–F) As in A, B and C using βGA instead of CBX. Note inhibition of EC $[Ca^{2+}]_i$ response to ACh with 100 μM βGA in F. *Significantly different from control, $P < 0.05$.

defined separation distances to provide a dynamic index of electrical conduction through GJCs (Hirst and Neild, 1978; Emerson and Segal, 2000a; Emerson *et al.*, 2002). In EC tubes, the relationship defined here between current injected at Site 1 and ΔV_m at Site 2 was linear ($R^2 \geq 0.99$) from ±0.1 to 3 nA (Figure 2B). Remarkably, hyperpolarization and depolarization were conducted equally along EC tubes with no evidence of rectification. This behaviour contrasts with electrical conduction along feed arteries of hamster skeletal muscle where, in response to ±0.8 nA microinjection, conduction of depolarization was only half as effective as the conduction of hyperpolarization (Emerson and Segal, 2000a). Nonlinearity of I-V relationships was also observed in guinea pig submucosal arterioles when ΔV_m exceeded 10 mV (Hirst and Neild, 1978). Our differences from previous studies may be explained by the absence of SMCs and their K_V channels to counteract depolarization in our EC tube preparations (Nelson and Quayle, 1995; Jackson, 2005; Kapela *et al.*, 2009). The linearity of I-V relationships at each distance (Figure 2B) highlights the endothelium as an electrical conduit that is indifferent to the polarity of charge movement and suggests a low functional expression of ion channels governed by voltage.

Our analyses of conduction amplitude evolved from 'slope resistance' (Hirst and Neild, 1978) and 'transfer resistance' (Emerson and Segal, 2000a) determined in previous studies. The linearity between current injected at Site 1 and ΔV_m at each distance (Figure 2B) enabled conduction amplitude to be calculated as ΔV_m in response to –1 nA. This value averaged 7–8 mV·nA^{-1} (Figure 2B, C) at a separation distance of 500 μm, which is consistent with values reported from hamster retractor feed arteries in response to –0.8 nA (Emerson and Segal, 2000a). Consistent with electronic decay, conduction amplitude decayed monoexponentially with a λ of 1.4 mm (Figure 2C). This value for λ is consistent with λ of 1.5 mm determined for isolated guinea pig arterioles (Hirst and Neild, 1978) and 1.2 mm for hamster feed arteries (Emerson *et al.*, 2002). Although SMCs were present in these earlier studies, the similarity of λ across preparations can be explained by the endothelium serving as the primary pathway for current flow, with minimal charge loss through myoendothelial GJCs attributable to the high input resistance of SMCs (Diep *et al.*, 2005).

We cannot exclude the possibility that active signalling events maintain a residual conduction amplitude (~3 mV·nA^{-1}) for distances beyond 2 mm, as electrical decay approached an asymptote beyond 1500 μm (Figure 2C). While this behaviour is consistent with findings in mouse cremaster muscle arterioles (Figueroa and Duling, 2008), the mechanism underlying the asymptote remains to be defined. As shown using cell expression systems, the conductance of GJCs can be governed by large (>20 mV) transjunctional voltage gradients between cell pairs expressing a single connexin isoform (Gonzalez *et al.*, 2007). However, native ECs express multiple connexin isoforms (Sandow *et al.*, 2003; Looft-Wilson *et al.*, 2004; Wolfle *et al.*, 2007) and it appears unlikely that a substantial voltage gradient occurs between neighbouring cells. As shown in Figure 2C, our determination of λ indicates a voltage gradient of ~8 mV over the distance of 2 mm (Figure 2C). Given individual ECs each ~35 μm in length within these tubes (Socha *et al.*, 2011), the voltage gradient between adjacent ECs would be <0.2 mV. These biophysical properties highlight the endothelium of resistance vessels as a highly effective electrical conduit with low resistance to the intercellular flow of current along the vessel axis.

Inhibition of intercellular coupling and hyperpolarization

The transfer of dye from one EC into neighbouring ECs (Figure 4) provides a qualitative index of intercellular coupling (Beny and Gribi, 1989; Welsh and Segal, 1998; Zhang *et al.*, 2006). The loss of dye coupling after 5 min treatment with CBX (Figure 4B) or βGA (Figure 4E) is consistent with the purported action of GA derivatives as inhibitors of GJCs (Yamamoto *et al.*, 1998; Tare *et al.*, 2002; Matchkov *et al.*, 2004; Dora *et al.*, 2008; Garland *et al.*, 2011). At the same time, electrical conduction along EC tubes in response to current injection was also abolished (Figure 3). Both CBX and βGA have been used to investigate endothelium-derived hyperpolarization and relaxation of vascular SMCs in response to ACh (Yamamoto *et al.*, 1998; Tare *et al.*, 2002; Matchkov *et al.*, 2004; Dora *et al.*, 2008; Garland *et al.*, 2011). Whereas inhibition of smooth muscle hyperpolarization and relaxation has been interpreted to reflect effects of GA derivatives on myoendothelial coupling through GJCs, it is difficult to locate their site(s) of action in the intact vessel wall.

GA derivatives exert non-selective actions on cells and tissues (Tare *et al.*, 2002; Rouach *et al.*, 2003; Matchkov *et al.*, 2004; Vessey *et al.*, 2004; Juszczak and Swiergiel, 2009). Thus, if GA derivatives inhibit signalling events integral to EC hyperpolarization, then electrical signalling from ECs to SMCs would be prevented, along with electrical conduction. Indeed, at concentrations shown to block endothelium-derived hyperpolarization and relaxation of arterial SMCs to ACh, both CBX (100 μM) and βGA (30 μM) suppressed hyperpolarization of ECs (Tare *et al.*, 2002). In the present study, hyperpolarization to ACh was impaired by concentrations of CBX (30 and 100 μM; Figure 5D) and βGA (10 and 30 μM; Figure 5H) that did not significantly alter EC $[Ca^{2+}]_i$ responses (Figure 7C, F). Such persistence of EC Ca^{2+} signalling during exposure to 100 μM CBX is consistent with findings in rat mesenteric arteries (Mather *et al.*, 2005). Whereas 100 μM CBX inhibited hyperpolarization to 3 μM ACh (Figure 5C) and to 1 μM NS309 (Figure 6F) in EC tubes, hyperpolarization to 1 μM ACh (ΔV_m averaged –9 mV from resting V_m of –52 mV) was maintained in ECs of rat mesenteric arteries (Dora *et al.*, 2008). Thus, while GA derivatives remain effective agents for reversibly inhibiting GJCs (Figure 4 and Supporting Information Figure S1), their non-specific actions may vary with the experimental preparation. Collectively, the present data illustrate the ability of GA derivatives to impair IK_{Ca}/SK_{Ca} channel activation, irrespective of actions on $[Ca^{2+}]_i$ signalling while also preventing dye transfer and electrical conduction through gap junctions (Figures 3–6). Whereas both GA derivatives increased baseline EC $[Ca^{2+}]_i$ (Figure 7B, E), the ability of βGA to suppress EC $[Ca^{2+}]_i$ responses to ACh (Figure 7D, F) suggests that its greater lipophilicity (relative to that of CBX) promoted access to the cell interior to influence internal Ca^{2+} stores.

In conclusion, our present findings have illustrated dynamic electrical conduction along freshly isolated EC tubes

from resistance arteries of mouse skeletal muscle. Resting V_m was less and the magnitude of hyperpolarization in response to ACh and NS309 was greater than typically reported for ECs studied in association with the vessel wall. Nevertheless, dye transfer between ECs and the electrical length constant along EC tubes were consistent with previous studies of intact arterioles and feed arteries. Remarkably, the amplitude and distance of electrical conduction along EC tubes were independent of charge polarity, suggesting that voltage-gated ion channels are poorly expressed within this endothelium. Either CBX or βGA effectively suppressed hyperpolarization to ACh or NS309 at concentrations equal to or lower than required to inhibit dye transfer, Ca^{2+} signalling or electrical conduction. We conclude that neither of these GA derivatives effectively distinguished the role of IK_{Ca}/SK_{Ca} channels from that of GJCs in defining electrical conduction along the endothelium.

Acknowledgements

We are grateful to Dr William F. Jackson for helpful discussion. This work was supported by the United States Public Health Service, National Institutes of Health grants R37-HL041026 and RO1-HL086483 (to SSS), F32-HL110701 (to EJB) and F32-HL107050 (to MJS).

Conflict of interest

None.

References

Alexander SPH, Mathie A, Peters JA (2011). Guide to Receptors and Channels (GRAC), 5th Edition. Br J Pharmacol 164 (Suppl. 1): S1–S324.

Bagher P, Segal SS (2011). Regulation of blood flow in the microcirculation: role of conducted vasodilation. Acta Physiol (Oxf) 202: 271–284.

Beny JL, Gribi F (1989). Dye and electrical coupling of endothelial cells in situ. Tissue Cell 21: 797–802.

Brondum E, Kold-Petersen H, Simonsen U, Aalkjaer C (2010). NS309 restores EDHF-type relaxation in mesenteric small arteries from type 2 diabetic ZDF rats. Br J Pharmacol 159: 154–165.

Busse R, Edwards G, Feletou M, Fleming I, Vanhoutte P, Weston A (2002). EDHF: bringing the concepts together. Trends Pharmacol Sci 23: 374–380.

Dalsgaard T, Kroigaard C, Misfeldt M, Bek T, Simonsen U (2010). Openers of small conductance calcium-activated potassium channels selectively enhance NO-mediated bradykinin vasodilatation in porcine retinal arterioles. Br J Pharmacol 160: 1496–1508.

Diep HK, Vigmond EJ, Segal SS, Welsh DG (2005). Defining electrical communication in skeletal muscle resistance arteries: a computational approach. J Physiol 568: 267–281.

Dora KA, Gallagher NT, McNeish A, Garland CJ (2008). Modulation of endothelial cell KCa3.1 channels during endothelium-derived hyperpolarizing factor signaling in mesenteric resistance arteries. Circ Res 102: 1247–1255.

Emerson GG, Segal SS (2000a). Electrical coupling between endothelial cells and smooth muscle cells in hamster feed arteries: role in vasomotor control. Circ Res 87: 474–479.

Emerson GG, Segal SS (2000b). Endothelial cell pathway for conduction of hyperpolarization and vasodilation along hamster feed artery. Circ Res 86: 94–100.

Emerson GG, Segal SS (2001). Electrical activation of endothelium evokes vasodilation and hyperpolarization along hamster feed arteries. Am J Physiol Heart Circ Physiol 280: H160–H167.

Emerson GG, Neild TO, Segal SS (2002). Conduction of hyperpolarization along hamster feed arteries: augmentation by acetylcholine. Am J Physiol Heart Circ Physiol 283: H102–H109.

Figueroa XF, Duling BR (2008). Dissection of two Cx37-independent conducted vasodilator mechanisms by deletion of Cx40: electrotonic versus regenerative conduction. Am J Physiol Heart Circ Physiol 295: H2001–H2007.

Garland CJ, Hiley CR, Dora KA (2011). EDHF: spreading the influence of the endothelium. Br J Pharmacol 164: 839–852.

Gonzalez D, Gomez-Hernandez JM, Barrio LC (2007). Molecular basis of voltage dependence of connexin channels: an integrative appraisal. Prog Biophys Mol Biol 94: 66–106.

Haas TL, Duling BR (1997). Morphology favors an endothelial cell pathway for longitudinal conduction within arterioles. Microvasc Res 53: 113–120.

Haug SJ, Segal SS (2005). Sympathetic neural inhibition of conducted vasodilatation along hamster feed arteries: complementary effects of α_1- and α_2-adrenoreceptor activation. J Physiol 563: 541–555.

Hirst GD, Neild TO (1978). An analysis of excitatory junctional potentials recorded from arterioles. J Physiol 280: 87–104.

Jackson WF (2005). Potassium channels in the peripheral microcirculation. Microcirculation 12: 113–127.

Juszczak GR, Swiergiel AH (2009). Properties of gap junction blockers and their behavioural, cognitive and electrophysiological effects: animal and human studies. Prog Neuropsychopharmacol Biol Psychiatry 33: 181–198.

Kansui Y, Garland CJ, Dora KA (2008). Enhanced spontaneous Ca2+ events in endothelial cells reflect signalling through myoendothelial gap junctions in pressurized mesenteric arteries. Cell Calcium 44: 135–146.

Kapela A, Bezerianos A, Tsoukias NM (2009). A mathematical model of vasoreactivity in rat mesenteric arterioles: I. Myoendothelial communication. Microcirculation 16: 694–713.

Larson DM, Kam EY, Sheridan JD (1983). Junctional transfer in cultured vascular endothelium: I. Electrical coupling. J Membr Biol 74: 103–113.

Lidington D, Ouellette Y, Tyml K (2000). Endotoxin increases intercellular resistance in microvascular endothelial cells by a tyrosine kinase pathway. J Cell Physiol 185: 117–125.

Looft-Wilson RC, Payne GW, Segal SS (2004). Connexin expression and conducted vasodilation along arteriolar endothelium in mouse skeletal muscle. J Appl Physiol 97: 1152–1158.

Matchkov VV, Rahman A, Peng H, Nilsson H, Aalkjaer C (2004). Junctional and nonjunctional effects of heptanol and glycyrrhetinic acid derivates in rat mesenteric small arteries. Br J Pharmacol 142: 961–972.

Mather S, Dora KA, Sandow SL, Winter P, Garland CJ (2005). Rapid endothelial cell-selective loading of connexin 40 antibody blocks endothelium-derived hyperpolarizing factor dilation in rat small mesenteric arteries. Circ Res 97: 399–407.

Nelson MT, Quayle JM (1995). Physiological roles and properties of potassium channels in arterial smooth muscle. Am J Physiol Cell Physiol 268: C799–C822.

Nilius B, Droogmans G (2001). Ion channels and their functional role in vascular endothelium. Physiol Rev 81: 1415–1459.

Rouach N, Segal M, Koulakoff A, Giaume C, Avignone E (2003). Carbenoxolone blockade of neuronal network activity in culture is not mediated by an action on gap junctions. J Physiol 553: 729–745.

Sandow SL, Tare M, Coleman HA, Hill CE, Parkington HC (2002). Involvement of myoendothelial gap junctions in the actions of endothelium-derived hyperpolarizing factor. Circ Res 90: 1108–1113.

Sandow SL, Looft-Wilson R, Doran B, Grayson TH, Segal SS, Hill CE (2003). Expression of homocellular and heterocellular gap junctions in hamster arterioles and feed arteries. Cardiovasc Res 60: 643–653.

Segal SS (2005). Regulation of blood flow in the microcirculation. Microcirculation 12: 33–45.

Segal SS, Jacobs TL (2001). Role for endothelial cell conduction in ascending vasodilatation and exercise hyperaemia in hamster skeletal muscle. J Physiol 536: 937–946.

Sheng JZ, Ella S, Davis MJ, Hill MA, Braun AP (2009). Openers of SK_{Ca} and IK_{Ca} channels enhance agonist-evoked endothelial nitric oxide synthesis and arteriolar vasodilation. FASEB J 23: 1138–1145.

Socha MJ, Hakim CH, Jackson WF, Segal SS (2011). Temperature effects on morphological integrity and Ca^{2+} signaling in freshly isolated murine feed artery endothelial cell tubes. Am J Physiol Heart Circ Physiol 301: H773–H783.

Strobaek D, Teuber L, Jorgensen TD, Ahring PK, Kjaer K, Hansen RS *et al.* (2004). Activation of human IK and SK Ca^{2+} -activated K^+ channels by NS309 (6,7-dichloro-1H-indole-2,3-dione 3-oxime). Biochim Biophys Acta 1665: 1–5.

Tare M, Coleman HA, Parkington HC (2002). Glycyrrhetinic derivatives inhibit hyperpolarization in endothelial cells of guinea pig and rat arteries. Am J Physiol Heart Circ Physiol 282: H335–H341.

Van Rijen H, van Kempen MJ, Analbers LJ, Rook MB, van Ginneken AC, Gros D *et al.* (1997). Gap junctions in human umbilical cord endothelial cells contain multiple connexins. Am J Physiol Cell Physiol 272: C117–C130.

Vessey JP, Lalonde MR, Mizan HA, Welch NC, Kelly ME, Barnes S (2004). Carbenoxolone inhibition of voltage-gated Ca channels and synaptic transmission in the retina. J Neurophysiol 92: 1252–1256.

Welsh DG, Segal SS (1998). Endothelial and smooth muscle cell conduction in arterioles controlling blood flow. Am J Physiol Heart Circ Physiol 274: H178–H186.

Wolfle SE, Schmidt VJ, Hoepfl B, Gebert A, Alcolea S, Gros D *et al.* (2007). Connexin45 cannot replace the function of connexin40 in conducting endothelium-dependent dilations along arterioles. Circ Res 101: 1292–1299.

Yamamoto Y, Fukuta H, Nakahira Y, Suzuki H (1998). Blockade by 18beta-glycyrrhetinic acid of intercellular electrical coupling in guinea-pig arterioles. J Physiol 511: 501–508.

Zhang Q, Cao C, Mangano M, Zhang Z, Silldorff EP, Lee-Kwon W *et al.* (2006). Descending vasa recta endothelium is an electrical syncytium. Am J Physiol Regul Integr Comp Physiol 291: R1688–R1699.

Zhang T, Wu DM, Xu GZ, Puro DG (2011). The electrotonic architecture of the retinal microvasculature: modulation by angiotensin II. J Physiol 589: 2383–2399.

Supporting information

Additional Supporting Information may be found in the online version of this article:

Figure S1 Partial inhibition of dye transfer by CBX and βGA. (A) Propidium iodide dye (0.1% in 2 M KCl microelectrode solution) was microinjected under control conditions during intracellular recording for 30 min. Note robust dye transfer to surrounding cells. (B) As in A, after 5 min pre-exposure to 30 μM CBX which was maintained during 30 min intracellular recording. Note reduced dye transfer. (C) As in A after 20 min washout of 30 μM CBX with PSS. Note restoration of dye transfer similar to control. (D) As described in A. (E) As in B using 10 μM βGA instead of CBX. Note reduced dye transfer. (F) As in C, with washout of 10 μM βGA with PSS. Note restoration of dye transfer similar to control.

Please note: Wiley-Blackwell are not responsible for the content or functionality of any supporting materials supplied by the authors. Any queries (other than missing material) should be directed to the corresponding author for the article.